

Subgrid-scale orography parametrization for HIRLAM - first experiments

Robert Sigg (SMHI), Laura Rontu (FMI), Kai Sattler (DMI)

1 Introduction

Today, surface orography influences the results of HIRLAM via explicitly resolved dynamics and parametrization of the surface momentum flux due to small-scale turbulence. This means that the only parameter determining the effects of the subgrid-scale orography is the orographic roughness. However, it is physically incorrect to describe mountain waves or flow blocking effects caused by the subgrid-scale obstacles by treating them as enhanced turbulence. Also, in an attempt to handle all mountain effects the orographic roughness parameter may be tuned to unrealistically large values. There is some evidence that the lack of proper subgrid-scale orography parametrization causes problems for the model and for the turbulence parametrization in particular. The need for an subgrid-scale orography parametrization in relation to subgrid-scale obstacles decreases as the model resolution grows well below 5-10 km. In this case the generation of all mountain waves is expected to be resolved with sufficient accuracy. However, wave dissipation might still need an additional parametrization. Thus, in the present versions of HIRLAM with a resolution coarser than 5-10 km a parametrization is needed to account for subgrid-scale orographic effects.

An additional problem is that the method of derivation of the orographic roughness in the present reference HIRLAM is not entirely correct. The values of orographic roughness should depend on the model resolution but the reference system of climate data generation uses a fixed resolution to determine this parameter. Also, specific orography-related problems arise with connection to the explicit dynamics. It has been shown that wave structures below about $3\Delta x$ are not handled correctly and may create additional noise for the model. Orographic features generating such waves should better be filtered out.

In this study the first results of implementing a subgrid-scale orography (SSO, often referred to as gravity-wave drag) parametrization are described. The scheme implemented is imported from Meteo France. Some background information about the scheme is given in Ch. 2 and the orography-related variables are discussed in Ch. 3. Diagnostic variables are presented in Ch. 4 while the results of a case study with the new scheme are analysed in Ch. 5. Some conclusions with proposals for further studies finish the report.

2 Meteo France SSO parametrization scheme

The subgrid-scale orography parametrization scheme of this study is the one used in the Arpege-Aladin forecast system. Documentation of the parametrization can be found in Cordoneanu and Geleyn (1998) and in the Arpege technical documentation (Geleyn (2000)). The parametrization includes the generation and dissipation of vertically propagating buoyancy waves, resonance effects and blocked-flow drag. The stress, $\vec{\tau} = (\tau_x, \tau_y)$, due to these physical processes is represented in the following way:

$$\vec{\tau}(x, y, z) = \gamma(x, y, z) \cdot \vec{\tau}_s(x, y) \quad (1)$$

where $\vec{\tau}_s$ represents the generation of wave stress related to buoyancy waves and the parameter γ determines the vertical distribution of wave stress. The latter includes wave breaking, modification due to resonance and blocked flow. The blocked-flow drag is normally regarded as a

separate physical process and not treated in the wave drag formulation (Lott and Miller (1997)). However, for simplicity it was adapted as a part of the wave flux calculations.

The generation of wave stress is calculated according to:

$$\vec{\tau}_s(x, y) = K_g \cdot \rho_s \cdot N_s \cdot \vec{V}_{fs} \cdot h_s \quad (2)$$

where K_g is a dimensionless tuning parameter set to $3.5 \cdot 10^{-3}$, ρ_s [kgm^{-3}] is the surface density, N_s [s^{-1}] is an effective Brunt-Väisälä frequency, \vec{V}_{fs} [ms^{-1}] is the fictive surface wind and h_s [m] is the standard deviation of orography. In order to calculate the fictive surface wind the anisotropy of the orography and the direction of the principal axis of the subgrid-scale obstacles with respect to the model grid are needed as well (see Ch. 3.3).

As long as there is no interaction between the vertically propagating buoyancy waves and the surroundings the associated wave stress is constant with height ($\gamma = 1$ in Eq. 1). At a certain level the wave amplitude becomes so large that the wave starts to break and a drag is exerted on the flow since wave energy is converted into small-scale turbulent motions. This level is referred to as the level of saturation. The level at which saturation takes place is calculated using a Richardson number concept. Above, the breaking process continues until a critical level is reached. From the saturation level up to a critical level (or to the top of the model if a critical level does not exist) the parameter γ (in Eq. 1) is modified linearly. In the parametrization, the critical level is defined as when the stratification becomes unstable or the wind has turned more than 90° . The parameter γ goes to zero when approaching the critical level and upwards from this level it is set to zero since the wave has been totally absorbed and the wave flux disappears. This process is schematically presented in Fig. 1.

In this parametrization waves may also reflect from the level of saturation. Maximum resonance occurs when the phase angle of the reflected wave is $\frac{3\pi}{2}$ while maximum destruction is present if the phase angle is $\frac{\pi}{2}$. The phase angle is determined by the height of the saturation level and the vertical wave length that depends on the wind velocity and stability of the flow.

If the obstacle is high enough a part of the flow becomes blocked. Blocking increases with increasing static stability and decreasing wind speed. A non-dimensional mountain height Fr_i (inverse Froude number) is defined as

$$Fr_i = N \frac{h}{U}, \quad (3)$$

where N is the Brunt-Väisälä frequency, U the wind velocity and h the mountain height. In the parametrization these are related to the surface parameters N_s , $|\vec{V}_{fs}|$ and h_s . The flow is assumed blocked if Fr_i is larger than a critical value Fr_{ic} (set to 0.5). The height of the blocked layer h_b is then obtained from

$$h_b = h \left(1 - \frac{Fr_{ic}}{Fr_i}\right), \quad (4)$$

The parameter γ (Eq. 1) is modified by a non-linear function from surface to the blocking height (Geleyn (2000)). The modifications of the wave drag due to wave reflection and flow blocking are schematically presented in Fig. 1.

3 Variables of HIRLAM related to orography

3.1 Surface geopotential

The surface geopotential is an important part of the lower boundary condition for the resolved model dynamics. It is derived from the average elevation on the model grid using constant

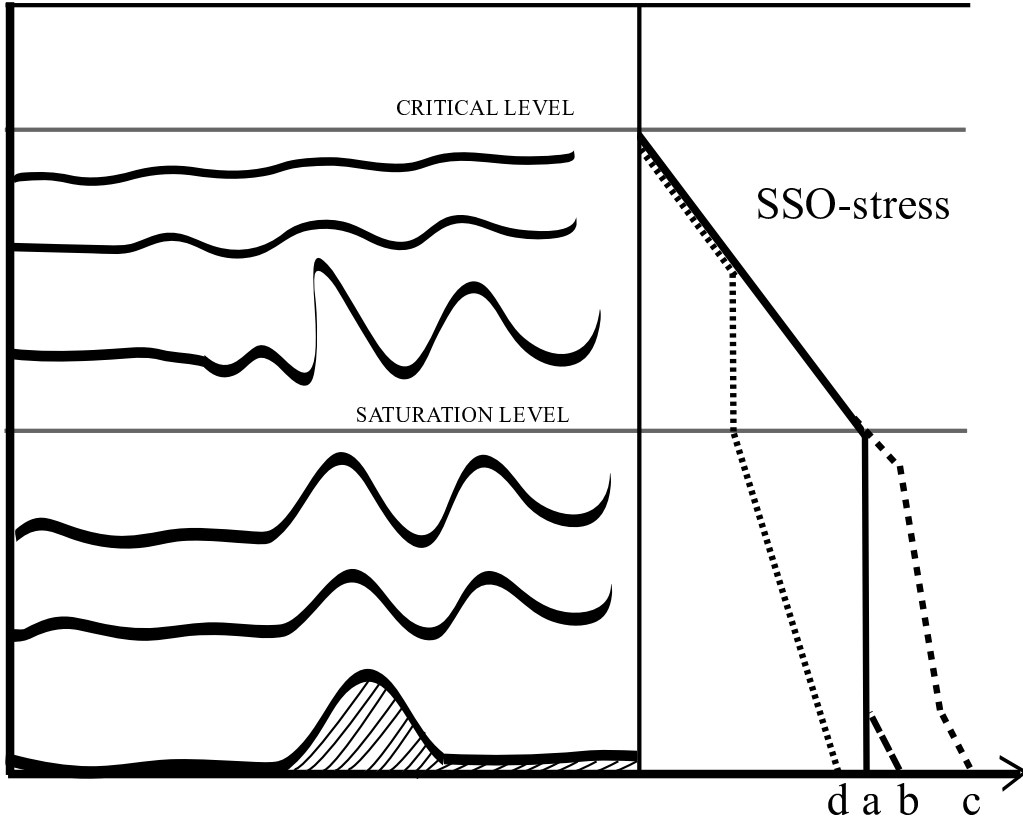


Figure 1: *Schematic picture of the wave breaking process. Idealized profiles of the parametrized SSO-stress are shown (a) for wave breaking only, (b) with flow blocking added, (c) for maximum resonance and (d) for maximum destruction due to wave reflection.*

gravity. The elevation is based on the GTOPO30" data (USGS (1998)). Because of its discretized formulation a finite difference model like HIRLAM does not resolve wave structures below $\lambda_h = 2\Delta x$ and tends to spuriously amplify $2\Delta x$ modes. Furthermore, it is not able to handle structures appropriately in the range between $2\Delta x$ and $3\Delta x$ due to aliasing effects (Raymond (1991)). In order to avoid a negative impact from orographic modes in this range, the averaged height field is filtered for structures with scales below approximately $3\Delta x$ using a Shapiro filter (Shapiro (1970)) (see also figure 2).

3.2 Orographic roughness

The roughness length is besides orography one of the most important parameters within the description of the model's lower boundary, because it has a direct influence on surface fluxes due to turbulence and their parametrization. There are two basic components influencing roughness length within the scope of the numerical model formulation: The first is roughness due to the land cover type, often referred to as vegetation roughness. It is not described in detail here. The second roughness component, $z_{0,oro}$, describes the impact of sub-grid orographic variations. It is derived from sub-grid orographic variance σ_{so}^2 and approximated empirically. The determination of σ_{so}^2 is based on the GTOPO30" data and thus includes variances beyond 30" resolution.

The present reference HIRLAM climate generation system (Bringfelt et al. (1995)) deter-

mines variance within a 23x23 pixel grid (corresponding to a horizontal scale of approximately 20 km), $\sigma_{so,23x23}^2$, as basis for the evaluation of $z_{0,oro}$, which is then scaled logarithmically:

$$z_{0,oro,ref} = a \left(\sigma_{so,23x23}^2 \right)^B. \quad (5)$$

The empirical scaling parameters a and B are in the current HIRLAM reference system $a = 0.4038$ and $B = 0.7767$.

A different approach is described by Sattler (1999), where an unscaled isotropic sub-grid orographic roughness length $z_{0,oro,unsc}$ is determined on basis of the grid dependend variance $\sigma_{so,A}^2$, which refers to the area A of the respective target grid square, and the number of relative height maxima n_p within this grid square. The approach uses a modified formulation, which goes back to Tibaldi and Geleyn (1981):

$$z_{0,oro,unsc} = \frac{1}{2} \sqrt{\frac{n_p + 0.001}{A}} \sigma_{so,A}^2. \quad (6)$$

The final sub-grid orographic roughness is then scaled analogously as before, i. e.

$$z_{0,oro,alt} = a \left(z_{0,oro,unsc} \right)^B, \quad (7)$$

where the empirical parameters are $a = 0.4038$ and $B = 0.715$. The final roughness field is filtered with a 4th-order gaussian filter in order to avoid possible sources for $2\Delta x$ -noise.

3.3 Parameters for the SSO scheme

The aggregation of the parameters related to sub-grid orography is done on a target grid, which has a lower resolution than the source grid, and which is rotated with respect to the source grid.

Definitions

There are three parameters representing sub-grid orography in the scheme. The first of them is the standard deviation of subgrid orography σ_{so} . The other two parameters describe the non-isotropic properties of sub-grid orography and are derived from the tensor of orographic gradient correlation (Lott and Miller (1997)):

$$H_{ij} = \frac{\overline{\frac{\partial h}{\partial x_i} \frac{\partial h}{\partial x_j}}}{\overline{\frac{\partial h}{\partial x_i} \frac{\partial h}{\partial x_i}}}. \quad (8)$$

h is the orography, as it is represented in the source grid, and x_i and x_j describe the coordinate axes of this grid. If we define

$$T = \frac{\partial h}{\partial x_i} \frac{\partial h}{\partial x_i} + \frac{\partial h}{\partial x_j} \frac{\partial h}{\partial x_j} \quad (9)$$

$$D = \sqrt{\left(\frac{\partial h}{\partial x_i} \frac{\partial h}{\partial x_i} - \frac{\partial h}{\partial x_j} \frac{\partial h}{\partial x_j} \right)^2 + 4 \left(\frac{\partial h}{\partial x_i} \frac{\partial h}{\partial x_j} \right)^2},$$

then the anisotropy value for use in the SSO parametrization is defined:

$$\gamma = \sqrt{\frac{|T - D|}{|T + D|}}. \quad (10)$$

Finally, the direction between the gradient of orography, as referred to the mean squares of the gradient components, and the x-axis of the model grid is defined:

$$\theta = \arctan \left(\frac{\frac{\partial h}{\partial x_j} \frac{\partial h}{\partial x_j} - \frac{\partial h}{\partial x_i} \frac{\partial h}{\partial x_i} + D}{2 \frac{\partial h}{\partial x_i} \frac{\partial h}{\partial x_j}} \right) \quad (11)$$

Source grid aggregation and filtering

The source orography is filtered in order to determine the subgrid-scale orography variables in a proper scale for the parametrization. Otherwise, the parametrization may simulate unrelated effects. The demands for the filter are, however, different from those from the model topography. Removal of both the higher and the lower spectrum seems appropriate here (Scinocca and McFarlane (2000)).

The smallest scale orographic structures (with a horizontal scale below a few kilometres) create turbulence but no mountain waves (Queney (1948)). It is thus appropriate to filter out smaller scales in the orography field using a low-pass filter. This is done by aggregating the orography from GTOPO30" onto a grid with approximately 2.7 km resolution. This grid is rotated at the same time in order to assure more homogeneity with respect to areal representation, which is necessary for the determination of σ_{so} .

In addition, the HIRLAM dynamics can be expected to resolve those scales in the orography, which are resolved in the (properly filtered) target grid. The properties of the high-pass filter should thus be consistent with the filter applied on the model orography, i. e. the filter should start to work where scales begin to be resolved by the model.

The following high-pass filter, which is based on a gaussian characteristics, was found to fulfill the demands from above:

$$h = h_L - [h_L]. \quad (12)$$

h_L denotes the low-pass filtered orography and $[h_L]$ is defined

$$[h_L(x)] = \frac{\int_{-\infty}^{\infty} g(x - x') h_L(x') dx'}{\int_{-\infty}^{\infty} g(x - x') dx'}, \quad (13)$$

where

$$g(x - x') = \exp \left(-\frac{2|x - x'|}{\delta} \right). \quad (14)$$

The scale parameter δ determines the area taken into account when determining $[h_L(x)]$. It is set to $\delta = 2\Delta x$, where Δx is the resolution of the target grid (model grid). The response function of the high-pass filter (12) is shown in figure 2 together with the response of the Shapiro filter used for the model orography, in order to show their behaviour within the transition zone of the wave spectrum. The lower x-axis denotes relative wave number with respect to the resolution of the low-pass filtered elevation Δh_L . The spectrum shown in the chart represents the complete spectrum of the h_L -orography. It extends from the long wave range at the left hand side to the short wave range up to $k/\Delta h_L = 0.5$, corresponding to $2\Delta x$ -waves in the h_L -grid, which represent the shortest possible waves in the low-pass filtered orography. The upper

x-axis denotes relative wave number with respect to the resolution of the target grid Δx . A value of $k/\Delta x = 0.3$ corresponds to $3\Delta x$ -waves with respect to the target grid. The transition between the two filters occurs approximately at this point. In the range $k/\Delta x > 0.5$ the sub-grid orographic structures occur. These are supposed to be important for SSO parametrization and are kept by the high-pass filter.

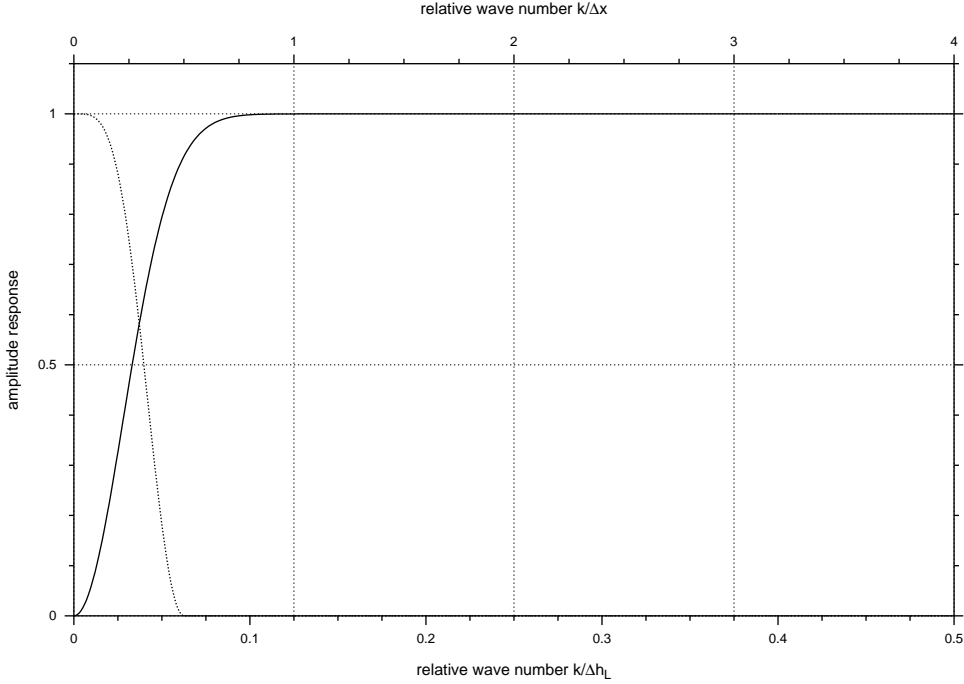


Figure 2: Response function of the Shapiro filter (dotted curve) used to filter model orography, and the high-pass filter (solid curve) used to filter the source orography for SSO parameter aggregation. Δx is chosen to $8\Delta h_L$ in the chart without loss of generality. See text for further details and a detailed description of the x-axis.

4 Diagnostics of the momentum budget in HIRLAM

The system of diagnostic variables in HIRLAM (Fortelius (2000), c.f. also Rontu and Fortelius (2000)) was used. The diagnosed tendencies of the horizontal wind $\vec{v}(x, y, z)$ consist of contributions from explicitly resolved dynamics (including in addition to advection also the influence of horizontal diffusion, corrections related to the numerical schemes, boundary relaxation, interpolations etc.) plus parametrized turbulence and subgrid-scale orography:

$$\frac{\partial \vec{v}}{\partial t} = \left(\frac{\partial \vec{v}}{\partial t}\right)_d + \left(\frac{\partial \vec{v}}{\partial t}\right)_p \quad (15)$$

$$\left(\frac{\partial \vec{v}}{\partial t}\right)_p = \left(\frac{\partial \vec{v}}{\partial t}\right)_t + \left(\frac{\partial \vec{v}}{\partial t}\right)_w \quad (16)$$

where the indexes d, p, t and w refer to dynamics, physics, turbulence and mountain waves, respectively. By definition, the turbulent and wave tendencies are related to vertical divergence

of corresponding subgrid-scale momentum fluxes or turbulent and wave stresses (defined here as forces exerted by the flow on the surface):

$$\left(\frac{\partial \vec{v}}{\partial t}\right)_t = \frac{1}{\rho} \frac{\partial \vec{\tau}_t}{\partial z}, \vec{\tau}_t = -\rho(\overline{v'w'})_t \quad (17)$$

$$\left(\frac{\partial \vec{v}}{\partial t}\right)_w = \frac{1}{\rho} \frac{\partial \vec{\tau}_w}{\partial z}, \vec{\tau}_w = -\rho(\overline{v'w'})_w, \quad (18)$$

where ρ is the air density, w is the vertical velocity, a prime ' denotes subgrid-scale deviation and overline gridbox average.

Integrating vertically we get

$$\widehat{\frac{\partial \vec{v}}{\partial t}} = \left(\widehat{\frac{\partial \vec{v}}{\partial t}}\right)_d + \left(\widehat{\frac{\partial \vec{v}}{\partial t}}\right)_t + \left(\widehat{\frac{\partial \vec{v}}{\partial t}}\right)_w = \left(\widehat{\frac{\partial \vec{v}}{\partial t}}\right)_d + \vec{\tau}_{ts} + \vec{\tau}_{ws}, \quad (19)$$

where a vertically integrated variable $\hat{x} = \int_0^{p_s} x \frac{dp}{g}$ is denoted by a hat and the index s refers to a surface value. The last part of Eq. (19) follows from the upper boundary condition defining that the subgrid-scale momentum fluxes vanish at the top of the atmosphere. Thus the vertically integrated tendencies of the horizontal wind due to the physical parametrizations reduces to contributions from turbulence and wave drag at the surface.

From the accumulated components of three-dimensional and vertically integrated tendencies of $\left(\frac{\partial u}{\partial t}\right)_p$, $\left(\frac{\partial u}{\partial t}\right)_t$, $\left(\frac{\partial v}{\partial t}\right)_p$ and $\left(\frac{\partial v}{\partial t}\right)_t$ all the components of the momentum budget due to physical parametrizations can be obtained. Change of the model state during the accumulation period gives the total tendency from which also the contribution of explicitly resolved dynamics can be calculated.

5 A case study

5.1 Description of the "Kiruna" case and model experiments

A case was selected with a westerly to northwesterly flow present over the Scandinavian Mountains. During the night of 26 January 2000 a cold front passed the mountain ridge and after the passage quite strong northwesterly winds swept down over the Northern Scandinavia (Fig. 3). This flow situation was quite steady until noon on 27 January when the winds decreased in strength and turned to the west. Mountain waves are usually generated under such flow conditions during wintertime. In order to detect any mountain wave activity a cross section along a straight line from Narvik in Norway to Kiruna in Sweden was examined (Fig. 3).

A 186x170 grid-point integration area defined for the Baltex/BRIDGE experiments was used for the model runs. The horizontal resolution was 22 km with 31 levels in the vertical. The experiments were made with the HIRLAM reference version 4.7.3 using initial and boundary data from ECMWF. Normal mode initialization technique, Eulerian dynamics with a time step of 90 sec, CBR turbulence and STRACO condensation were used. The HIRLAM simulation time was 36 hours beginning at 18 UTC on January 25 2000.

Five different model setups were investigated in this study. The reference run (KRF) was performed with the reference version 4.7.3 while the other model configurations (KZF, KFF, K2F, K3F) were based on this but modified according to the table.

At present, surface roughness has been calculated with an algorithm that seems to overestimate the surface roughness in mountain regions. Therefore, surface roughness has been re-calculated according to a grid-size dependent method (Ch 3.2). This implies that the new

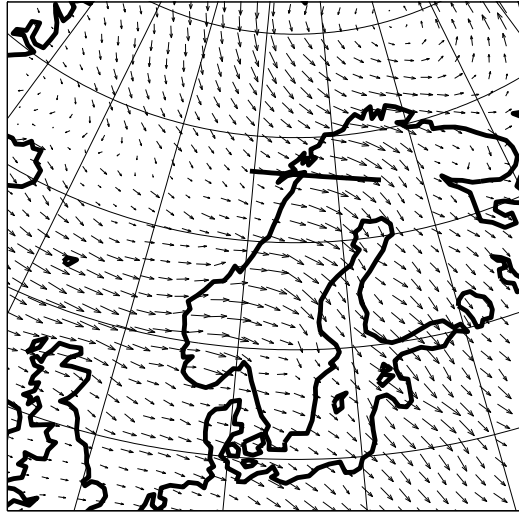


Figure 3: *The dynamic situation over Scandinavia at 06 UTC on January 27. The investigated cross section is indicated with the black full line.*

surface roughness values are about half in magnitude of the old ones for the northern Scandinavian Mountains (Fig. 4a). The new surface roughness has maximum values of one metre in this area while the old roughness reaches more than two metres.

The surface geopotential of the reference HIRLAM system is unfiltered. In this study it was filtered for structures with scales below $3\Delta x$ (Ch. 3.3). The filtering clearly influences the appearance of the mountains along the chosen cross section (Fig. 4b). The mountain top and the hill before the main mountain ridge are slightly lower. Both downstream and upstream the mountain oscillating features are smoothed out.

The difference between filtered and unfiltered sub-grid scale orography variables (Ch. 3.3) shown in Fig.5 is relatively small along the cross section. The largest differences occur upstream the mountain ridge where both the filtered standard deviation and the filtered anisotropy are larger than the unfiltered values.

5.2 Model results and discussion

The main dynamic feature with northwesterly winds over northern Scandinavia is captured by all model configurations. The mountain generates a resolved buoyancy wave present in all model runs indicated by the isentropes along the chosen cross section. Maximum turbulent kinetic energy (TKE) is produced by the turbulence parametrization scheme over the main mountain ridge (Fig. 6a). There the maximum TKE value is close to $3 m^2 s^{-2}$ and elsewhere near the surface it is of the order of $1 m^2 s^{-2}$. Upstream the mountain the boundary layer is about 1.5 km deep while it collapses downstream the ridge and is only a couple of hundred meters in depth. The resolved mountain wave is associated with strong downslope winds with a maximum close to $20 m s^{-1}$ above and downstream the mountain ridge. The observations of synoptic stations indicate that these values are realistic. Boundary-layer friction causes a strong retardation of the incoming northwesterly flow as indicated by the negative accumulated u-momentum tendencies (Fig. 6b). Only u-momentum tendencies are analysed since the cross section is oriented along the model's x-axis. The retardation follows the shape of the terrain with the maximum values located over the ridge, where the orographic roughness is large.

When the modified orographic roughness is used (KZF) the accumulated u-momentum tendencies are reduced by approximately 20 % over the mountain ridge (Fig. 7a) and the flow

Table 1: Definition of the Kiruna experiments

	KRF	KZF	KFF	K2F	K3F
Re-calculated orographic roughnes	no	yes	yes	yes	yes
Low-pass filtered surface geopotential	no	no	yes	yes	yes
High-pass filtered SSO	-	-	-	no	yes

is therefore less retarded. The downslope wind speed maximum is not changed significantly. Similar patterns are also present both in the experiment with smoothed surface geopotential (KFF, Fig. 7b) and when the SSO parametrization is added (K2F, Fig. 7c). Downstream the ridge it seems that the u-momentum field is smoother in the KFF experiment than in the other runs. This might be an indication that the SSO parametrization restores the irregularities that were lost when a smoother surface geopotential was introduced.

The accumulated u-momentum tendencies due to the SSO parametrization is shown in Fig. 8a. Apparently, wave breaking takes place at the heights of 12-15 km and 20-25 km. The strongest drag with two maxima is correlated with the maximum values of the standard deviation over the mountain ridge (Fig. 5a). This means that the wave drag generated near the surface is influencing the flow at upper levels which seems realistic since wave breaking usually takes place at high altitudes. However, the role of possible wave reflection from the model's upper boundary and its interaction with the SSO parametrization remains to be studied.

At the surface and on the upstream side of the mountain flow blocking is present (not seen in Fig. 8a due to the chosen vertical scale). In this flow situation the blocking effect is small, with a magnitude of the order of 1 % of the boundary-layer turbulence effect.

When using the filtered SSO parameters only small differences are present compared with the previous run (Fig. 8b). Wave breaking takes place at similar altitudes as before and flow blocking is present on the upstream side of the mountain ridge. The largest difference is in the accumulated u-momentum tendencies on the upstream side of the mountain at high altitudes. There is less drag in the K3F run, which is consistent with the smaller standard deviation in this area (the second peak in Fig. 5a). Further investigation is needed to choose optimal filtering of the SSO.

The accumulated momentum tendencies were integrated vertically to obtain the surface stress produced by the SSO parametrization (Eq. 19). The difference of the total (turbulent plus wave) stress between the reference HIRLAM and the experiment with unfiltered SSO parameters (Fig. 9) shows the combined effect of the new parametrization and related changes of the orography fields. The magnitude of the retarding force given by the experiment with the SSO parametrization is smaller than that of the reference experiment over the main mountain ridge and greater on the downstream side. Thus, buoyancy waves can only partly compensate for the loss of drag due to the reduced orographic roughness over the mountain ridge. More experiments and tuning are needed to find and define the correct relations between the SSO and turbulence parametrizations. At the cover picture of this Newsletter there is an example of the distribution of the surface wave stress vector indicating that quite large mountain areas are influenced by the

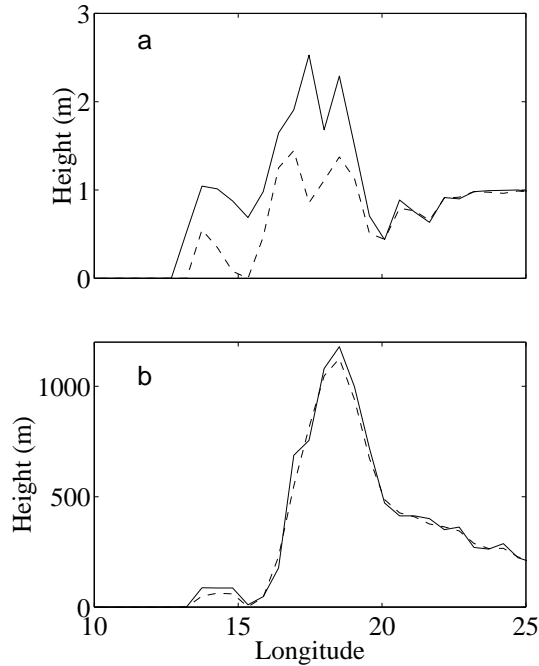


Figure 4: (a) Surface roughness along the cross section for the reference HIRLAM (full) and the re-calculated values (dashed). (b) Unfiltered (full) and filtered (dashed) surface geopotential along the same cross section.

SSO parametrization. The order of magnitude of the wave-induced surface stress over mountain areas shown in the picture is on average about one order of magnitude smaller than the turbulent stress.

6 Summary and conclusions

In this study a subgrid-scale orography (SSO) parametrization was implemented into HIRLAM. The scheme is identical to the gravity-wave parametrization scheme of the Arpege-Aladin forecast system. This parametrization is capable of handling the generation and the dissipation of sub-grid scale buoyancy waves in mountain regions. The vertically propagating buoyancy waves break when they reach the saturation level and deposit momentum from this level to the critical level. Thus, a drag is exerted on the mean flow due to this process. Also included in the parametrization are the influence of resonance effects on the flux of wave momentum and flow blocking.

In order for the SSO parametrization to work new orography variables were generated: standard deviation of mean orography (sub-grid scale orography), anisotropy and the angle between the direction of the x-axis of the model grid and the principal axis of the orography. Two setups of such variables were experimented with, unfiltered and filtered ones. The filtering process removed the influence of larger scales on the SSO variables.

Surface roughness was re-calculated with a grid-size dependent algorithm since the reference HIRLAM calculations seem to overestimate the surface roughness in mountain regions. This modification reduced surface roughness to approximately half the old values. In addition, the surface geopotential was filtered for scales below $3\Delta x$ to avoid generation of numerical noise. Thus, the runs with the SSO parametrization included were performed with modified surface roughness and filtered surface geopotential. Additional runs were made to investigate the effects

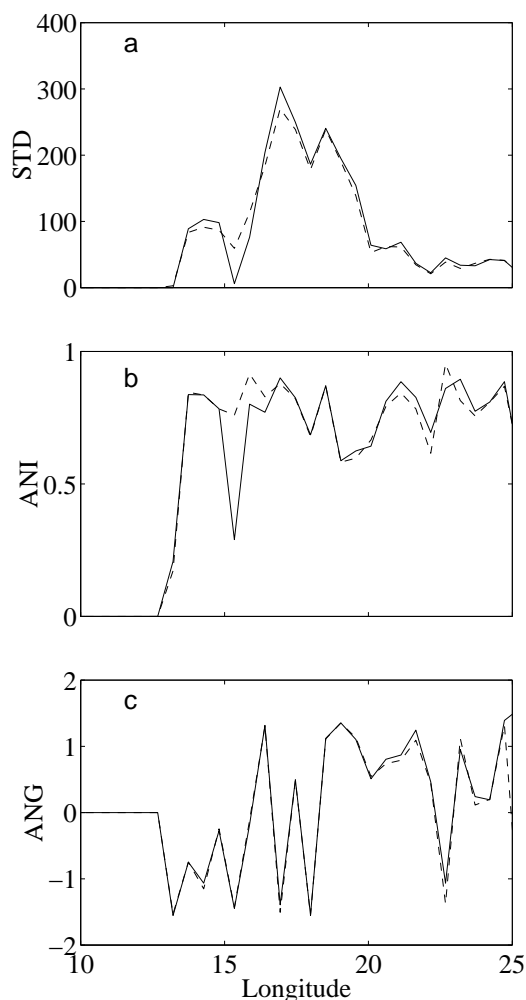


Figure 5: (a) Unfiltered (full) and high-pass filtered (dashed) standard deviation of orography along the cross section with similar comparisons for (b) the anisotropy and (c) the angle between the direction of the model's x -axis and principal axis of the orography.

of the orography modifications only.

A case was selected with northwesterly winds sweeping down over northern Scandinavia behind a cold front that passed during the night of 26 January 2000. The main dynamic situation is well simulated by HIRLAM and boundary-layer friction causes a strong retardation of the incoming northwesterly flow. When reducing the surface roughness the retardation is reduced while the implementation of filtered mean orography has little effect on the mean flow and the retardation.

The SSO drag does not influence the mean flow significantly at lower altitudes (below 5 km height) except for some flow blocking which is small in this case. However, vertically propagating buoyancy waves are generated on the sub-grid scale and they break at higher altitudes. With wave drag included a more physical behaviour of the drag profile is therefore achieved. The drag from buoyancy waves can partly compensate for the loss of the drag due to orographic roughness. The sum of the turbulent and wave drag at the surface is changed with more drag mainly downstream the main mountain ridge. However, at the main ridge the drag from buoyancy waves is not large enough to compensate for the loss of turbulent drag. There are

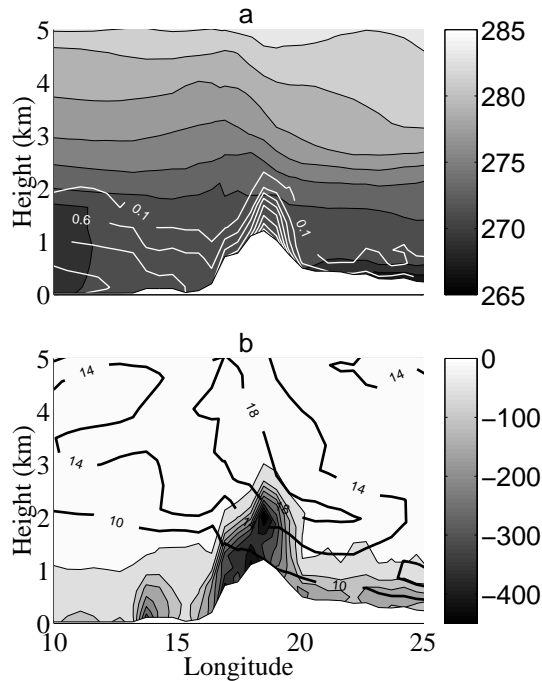


Figure 6: *Flow characteristics according to the reference (KRF) experiment, 36h forecast based on the analysis at 18UTC, January, 25. (a) Potential temperature (black) and turbulent kinetic energy (white) along the cross section. Contour lines every 4 K and $0.5 \text{ m}^2\text{s}^{-2}$, respectively. (b) Accumulated u -momentum tendencies together with the u -wind (full black, larger than 10 ms^{-1}). Contour lines are drawn every 20 ms^{-1} and 4 ms^{-1} , respectively.*

small differences in the runs with unfiltered and high-pass filtered SSO orography.

The plans are to continue to investigate the effects of the SSO parametrization with different horizontal resolutions (0.1° , 0.2° and 0.4°). Further studies are needed to choose optimal filtering of the subgrid-scale orography. Longer runs with data assimilation will be performed in order to deduce systematic pressure differences in mountain regions between runs with and without the SSO drag. These runs should also allow to study the interaction between the turbulence and SSO parametrizations in order to tune the schemes. Also, extra model levels will be added to HIRLAM at high altitudes to test the ability of the scheme to handle the wave breaking in the stratosphere and to reveal the effects of the formulation of the model's upper boundary condition. Studies using both the non-hydrostatic and hydrostatic HIRLAM are planned with emphasis on resolved mountain waves.

Acknowledgements

The authors would like to thank Michael Tjernström and Per Källberg for their work with the HIRLAM-Arpege interface. Also thanks to Jean-Francois Geleyn and Eric Bazile at Meteo France who kindly answered all our questions related to the present parametrization. Guidance from Carl Fortelius helped us to define diagnostic tools for this study. In addition, we appreciate the comments from Per Undén on the work and the manuscript.

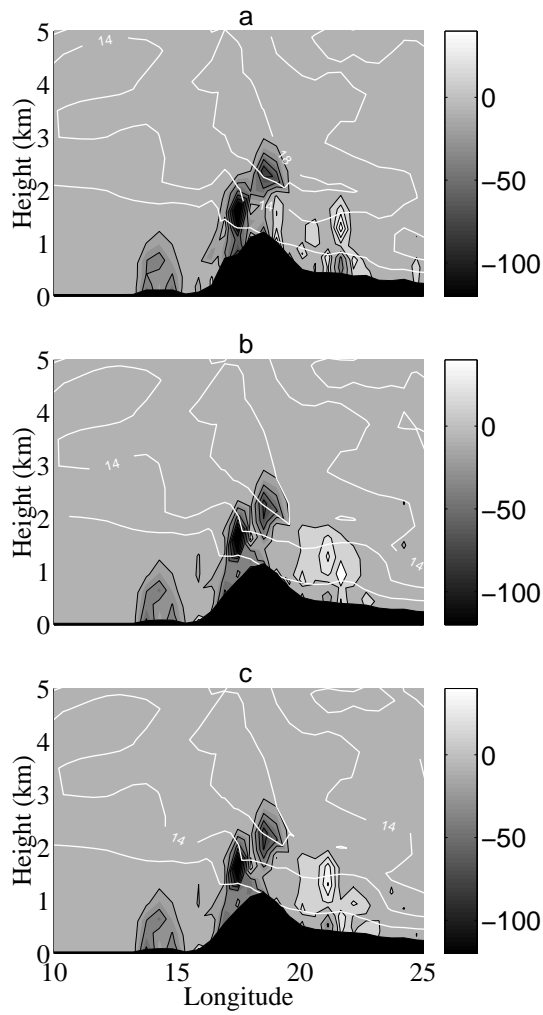


Figure 7: *The difference of the total accumulated u -momentum tendencies between the reference run and three experiments: (a) KRF-KZF, (b) KRF-KFF, (c) KRF-K2F together with the u -component of wind (white) from corresponding experiments. Contour lines are 20 (negative values) and 10 (positive values) ms^{-1} . Wind is contoured as in Fig. 6b*

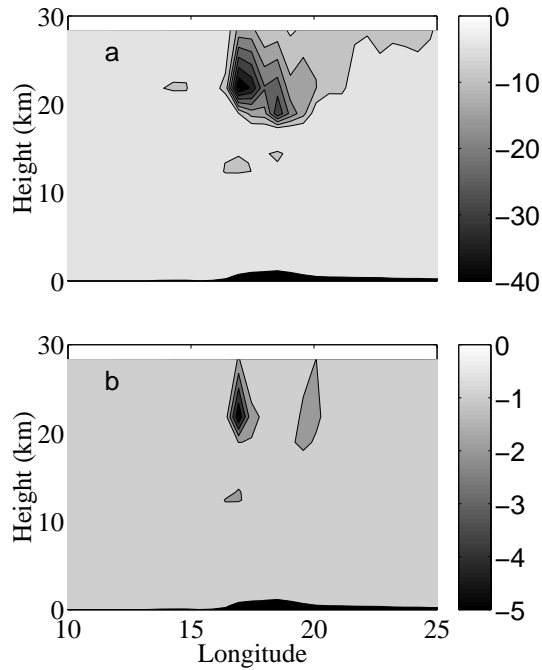


Figure 8: (a) The accumulated u -momentum tendency due to the SSO parametrization (experiment $K2F$) and (b) the difference between the experiments using unfiltered and high-pass filtered SSO ($K2F-K3F$). The contour lines are drawn every 5 and 1 ms^{-1} , respectively.

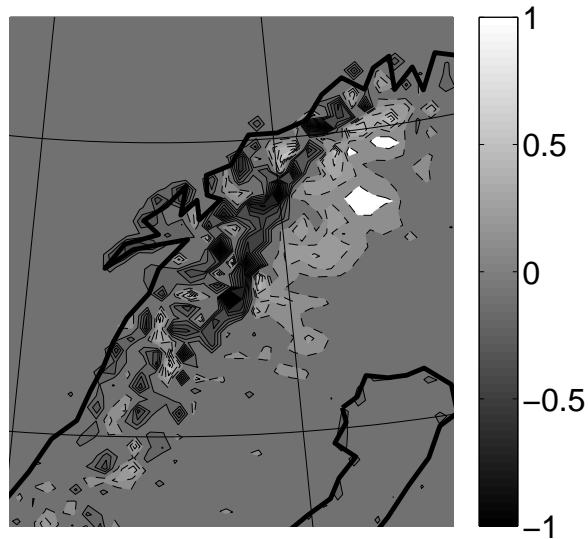


Figure 9: The difference of vertically integrated total accumulated u -momentum tendencies (accumulated over 36h) with and without the SSO drag ($KRF-K2F$). There are mainly negative values (full) over the mountain ridges and positive values (dashed) around. Contour lines are drawn with an interval of $10^4 \text{ Nm}^{-2}\text{s}$

References

- Bringfelt, B., N. Gustafsson, P. Vilmusenaho and S. Järvenoja, 1995: Updating of the HIRLAM physiography and climate data base. Hirlam Technical Report, 19. Norrköping, June 1995, 42 pp.
- Cordeneanu, Elena and J.-F. Geleyn, 1998: Application to local circulations above the Carpathian-Black sea area of a NEP-type meso-scale model. *Contr. Phys. Atmos.*, **71/2**, 191-212.
- Fortelius, C., 2000: Status of the HIRLAM delayed mode data assimilation for BAL-TEX/BRIDGE. *Hirlam Newsletter*, **35**, 2000, 193-198.
- Rontu, L. and C. Fortelius, 2000: Recent developments in postprocessing. *Hirlam Newsletter*, **36**, 2000, 80-88.
- Geleyn J.F., 2000: Arpege technical documentation. Available at Meteo France, Toulouse. (<http://www.cnrm.meteo.fr/aladin/MODELES/EXT/Physics/>).
- Lott, F. and Miller M.J., 1997: A new subgrid-scale orographic drag parametrization: Its formulation and testing. *Q.J.Roy.Met.Soc.*, **123**, 101-127.
- Queney, P., 1948: The problem of air flow over mountains: A summary of theoretical studies. *Bull. Am. Met. Soc.*, **29**, 16-25.
- Raymond, W.H., 1991: A Review of Recursive and Implicit Filters. *Mon. Wea. Rev.*, **119**, 477-495.
- Sattler, K., 1999: New high resolution physiographic data and climate generation for the HIRLAM forecasting system. *DMI Technical Report*, **99-11**, 1999, 41pp.
- Scinocca, J.F. and McFarlane, N.A., 2000: The parametrization of drag induced by stratified flow over anisotropic orography. *Q.J.Roy.Met.Soc.*, **126**, 2353-2393.
- Shapiro, R., 1970: Smoothing, Filtering and Boundary Effects. *Rev. Geophys. and Space Phys.*, **8**, 359-387.
- Tibaldi, S., Geleyn, J.-F., 1981: The Production of a new Orography, Land-Sea Mask and associated Climatological Surface Fields for Operational Purposes. ECMWF Research Department Tech. Memorandum, 40, 13 pp + Appendices and Figures.
- USGS 1998: GTOPO30, Global 30 Arc Second Elevation Data Set. *U.S. Geological Survey*, <http://edcdaac.usgs.gov/gtopo30/gtopo30.html>